Polymer 49 (2008) 2857–2865

Contents lists available at ScienceDirect

Polymer

journal homepage: www.elsevier.com/locate/polymer

The bulk polymerisation of *N*-vinylcarbazole in the presence of both multi- and single-walled carbon nanotubes: A comparative study

Arjun Maity, Suprakas Sinha Ray*, Mpitloane J. Hato

National Centre for Nano-Structured Materials, Council for Scientific and Industrial Research, 1-Meiring Naude Road, Brummeria, P.O. Box 395, Pretoria 0001, South Africa

ARTICLE INFO

Article history:
Received 16 November 2007
Received in revised form 15 April 2008
Accepted 15 April 2008
Available online 18 April 2008

Keywords:
N-Vinylcarbazole
Carbon nanotubes
Polymerisation

ABSTRACT

The bulk polymerisation of *N*-vinylcarbazole (NVC) at an elevated temperature in the presence of both multi- and single-walled carbon nanotubes (CNTs) leads to the formation of two different types of composite materials, the morphology and properties of which were characterised by a field emission scanning electron microscopy (FE-SEM), Fourier transform infrared (FTIR) spectroscopy, Raman spectroscopy, X-ray photoelectron spectroscopy (XPS), thermogravimetric analysis, and electrical property measurements. The efficiency of CNTs to initiate the NVC polymerisation was investigated using both multi-walled CNTs (MWCNTs) and single-walled CNTs (SWCNTs). The focus was on three major aspects: the degree of polymerisation, the morphology and the properties of the resulting nanocomposite materials. Results showed that SWCNTs were more efficient in initiating NVC polymerisation than MWCNTs, and the morphology of resultant nanocomposites revealed wrapping and grafting of some poly(*N*-vinylcarbazole) (PNVC) chains on the SWCNT surfaces. The morphology of the PNVC/MWCNT nanocomposites showed only homogeneous wrapping of the outer surfaces of MWCNTs by PNVC chains. The direct current (dc) electrical conductivity of pure PNVC improved dramatically in the presence of both MWCNTs and SWCNTs, however, the extent of improvement is higher in the case of PNVC/MWCNT nanocomposites.

1. Introduction

In the family of speciality polymers such as poly(*N*-vinylcarbazole) (PNVC), polyaniline (PANI), polypyrrole (PPY), polythiophene (PTP), etc., PNVC is well known for its exceptionally high thermal stability, high photoconductivity and opto-electronic properties [1,2]. However, the very low dc conductivity (in the range of 10^{-12}–10^{-16} S/cm) of PNVC is frequently not good enough for various end-use applications.

During the last decade, numerous attempts have been made to chemically modify PNVC homopolymer to produce potential materials with improved electrical and other properties [3]. Due to their unique structure and properties, carbon nanotubes (CNTs) (SWCNTs and MWCNTs) have been investigated for various potential applications [4–8]. Their fascinating electrical and electronic properties, particularly, offer a new arena for the development of advanced functional materials based on functional polymer matrices.

It has also been established that CNTs could exhibit an amphoteric behaviour by exchanging electrons with electron acceptors, or electron donors, to form the corresponding positive or negative-charged counterions [9–12].

Against this background, the incorporation of CNTs into the PNVC matrix to prepare PNVC/CNT nano-structured materials may be one of the best ways to improve the properties of PNVC concurrently. In this context, several research groups have reported on the preparation and characterisation of various types of PNVC/CNT nanocomposites [13–19]. For example, a novel material of PNVC/functionalised SWCNTs was prepared through nucleophilic reaction, which exhibited large optical limiting effects due to photoinduced electron-transfer interaction [13]. The electron spin resonance (ESR) spectrum of the PNVC/SWCNT composites revealed two new signals and these were attributed to photoinduced interaction between PNVC and SWCNTs. The PNVC/MWCNT composites were fabricated for optical limiting behavioural measurement [14]. The observed optical limiting performance is mainly due to nonlinear absorption. The bounded polymer, with strong electron donating ability, can increase the intramolecular electron transfer and thus heighten the delocalisation of the π-conjugated system and probably improve the nonlinearities of CNTs. Furthermore, the nature of the charge transfer between the polymer and CNTs is demonstrated by ESR spectra [15]. The novel PNVC/SWCNT composite devices were fabricated applying a combination of laser ablation and the cluster-beam deposition method [16]. Wu et al.

* Corresponding author. Tel.: +27 12 841 2388; fax: +27 12 841 2135.
E-mail address: rsuprakas@csir.co.za (S. Sinha Ray).

0032-3861/$ – see front matter © 2008 Elsevier Ltd. All rights reserved.
doi:10.1016/j.polymer.2008.04.027

prepared PNVC/MWCNT blends by solvent casting using $CHCl_3$ as a co-solvent to study the effect of the incorporation of CNTs on the photoconductivity of PNVC [17]. In another procedure, PNVC/SWCNTs' nanocomposite thin film was obtained by spin-coating, using toluene as solvent [18]. PNVC/CNT nanocomposites were also synthesised by the electrochemical polymerisation technique [19].

In recent years, many researchers have used various methods for the preparation of PNVC/CNT nanocomposites, however, nobody have checked the ability of CNTs to initiate the *in situ* polymerisation of NVC monomers and fabrication of PNVC/CNT nanocomposites in the polymerisation system. In recent communication, we have for the first time reported on the *in situ* initiation of NVC polymerisation in the presence of MWCNTs at an elevated temperature. Field emission scanning and transmission electron microscopic observations showed the homogeneous wrapping of the MWCNT outer surfaces by PNVC polymer [20].

The main objective of this article is to report on the efficiency of CNTs to initiate NVC polymerisation. Both SWCNTs and MWCNTs were used for the preparation of nanocomposites with PNVC and the concentration of CNTs was kept at a very low level to understand the efficiency of CNTs in the initiation of NVC bulk polymerisation. Morphology and properties of pure CNTs, PNVC, and PNVC/CNT nanocomposites were extensively investigated in the Fourier transform infrared (FTIR) spectroscopy, field emission scanning electron microscopy (FE-SEM), Raman spectroscopy, X-ray photoelectron spectroscopy (XPS), and in thermogravimetric analysis (TGA). dc electrical conductivity of pure polymer and nanocomposites was also measured. On the basis of these results, a general understanding on the role of CNTs to initiate NVC bulk polymerisation is described and it is explained why two different types of CNTs-based polymerisation systems show different types of morphology and properties.

2. Experimental part

Prior to use, NVC monomers (Sigma–Aldrich Chemicals, SA) were re-crystallised from *n*-hexane and stored in a dark place. Both the MWCNTs and SWCNTs used in this study were synthesised in the laboratory by chemical vapour deposition (CVD) and laser ablation methods, respectively. Both the CNTs were preheated at 120 °C for 2 h before use. All other solvents used were of analytical grade and freshly distilled before use.

Nanocomposites were synthesised *via in situ* solid-state polymerisation of monomers in the presence of CNTs at an elevated temperature without any external oxidant. In a typical polymerisation system, a mixture of known weight (0.5 g) of NVC and a known amount of MWCNTs (0.05 g) was taken in a conical flask and heated at 70 °C (above the melting temperature of the NVC monomer, mp 65 °C) for 1.5 h. Distilled tetrahydrofuran (THF, 5 ml) was added into the reaction mixture and stirred for 2 h. The whole reaction mixture was poured into an excess of methanol (MeOH). The precipitating greyish black mass, i.e. PNVC/MWCNT nanocomposites, was filtered and washed with boiling MeOH to remove any unreacted monomer and followed by washing with acetone [21]. The obtained mass was dried at 100 °C for 6 h, under vacuum, until the total mass became constant. The PNVC/SWCNTs' nanocomposite was also prepared by the same procedure using SWCNTs instead of MWCNTs.

To extract PNVC homopolymer from the nanocomposite samples, the dried nanocomposites (PNVC/MWCNTs and PNVC/SWCNTs nanocomposites) were refluxed with 20 ml benzene (benzene is a good solvent for PNVC homopolymer) at 70 °C for 48 h. Thereafter, the solution was poured into an excess of MeOH to yield a white precipitate, i.e. PNVC homopolymer. The white mass was filtered and washed with boiling MeOH, followed by acetone, and finally dried at 100 °C overnight until constant weight was obtained. For comparison purpose, PNVC homopolymer was also prepared using $FeCl_3$, as an oxidant.

The formation of PNVC in the presence of both CNTs and its presence in the nanocomposite samples were confirmed by Attenuated Total Reflectance (ATR) Fourier transform infrared (FTIR) spectroscopy, using a Perkin–Elmer Spectrum 100 spectrometer equipped with an IR microscope accessory and a germanium crystal. The morphology of the various samples was studied by means of FE-SEM (LEO, Zeiss). The purity of CNTs was evaluated by means of the high resolution transmission electron microscope (HR-TEM) (JEOL JEM 2100F), operated at an accelerated voltage of 200 kV. To obtain more information on the wrapping and/or the grafting of PNVC polymer chains on the CNT outer surfaces, Raman spectra of MWCNTs, SWCNTs and their nanocomposites with PNVC were recorded by a Lab Raman system (Jobin-Yvon Horiba T64000 spectroscope) equipped with an Olympus BX-40 microscope. The excitation wavelength was of 514.5 nm with an energy setting of 1.2 mW from a Coherent Innova Model 308 argon ion laser. Elemental mapping of CNTs, PNVC, and nanocomposite samples was performed, using an X-ray photoelectron spectroscope (XPS) on a Kratos Axis Ultra device, with an Al monochromatic X-ray source (1486.6 eV). Survey spectra were acquired at 160 eV and region spectra at 20 eV pass energies, respectively. The thermal stability of the samples was investigated, using a TGA Q500 instrument (TA instrument) at a heating rate of 10 °C/min under nitrogen (N_2) atmosphere (flow rate 50 ml/min). The dc conductivity was measured by a four-probe method (Keithley, USA) at room temperature with a programmable dc voltage/current detector. The data shown here represent the mean measurement values from at least three samples.

3. Results and discussion

To use CNTs as precursors for the NVC polymerisation, it is important to know the purity of the CNTs. The FE-SEM images of purified CNTs are shown in Fig. 1. Parts (a) and (b) of Fig. 2, respectively, represent the energy dispersive X-ray (EDX) spectra of MWCNTs and SWCNTs. It is clear from the FE-SEM image and EDX spectra that MWCNTs used in this study were very pure and no catalyst, originally used for the synthesis of MWCNTs, was present. However, the EDX spectra of the SWCNTs show the presence of a very small amount of elemental nickel (Ni) and cobalt (Co). It has also already been proved that metals in elemental form have no effect on the polymerisation of the NVC monomers. To support the FE-SEM results and EDX spectra, HR-TEM analyses were conducted to directly and qualitatively visualise the purity of both the CNT samples. Parts (a) and (b) of Fig. 3, respectively, show the HR-TEM images of MWCNTs and SWCNTs which correspond to the FE-SEM images and EDS spectra as shown in Figs. 1 and 2. The HR-TEM image of MWCNTs reveals that the tubes are very pure, whereas the HR-TEM image of SWCNTs shows the presence of some fullerenes or amorphous carbon materials. It is very difficult to see the presence of catalyst particles. Therefore, on the basis of these results, one can conclude that the initiation of NVC polymerisation by CNTs is not due to the presence of catalyst particles or other impurities.

The formation of PNVC polymer in the presence of both CNTs and its presence in the nanocomposite samples were examined by ATR-FTIR spectroscopic studies. Fig. 4 represents the ATR spectra of PNVC synthesised by oxidant ($FeCl_3$), PNVC extracted from nanocomposites, and two different nanocomposite samples. The IR peak positions and their probable assignments are described in Table 1. Results of Fig. 4 and Table 1 prove the ability of both CNTs to promote *in situ* polymerisation of NVC monomers at an elevated temperature.

To check the effect of temperature on the NVC polymerisation, an experiment was done under the same conditions, but in the

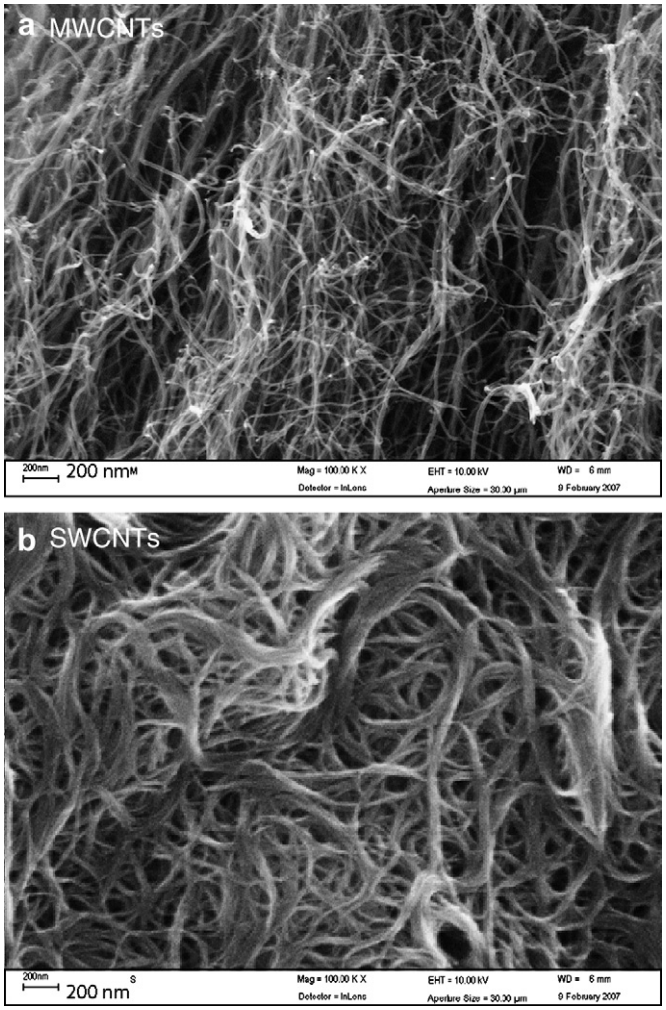

Fig. 1. Field emission scanning electron microscopic images of (a) MWCNTs and (b) SWCNTs.

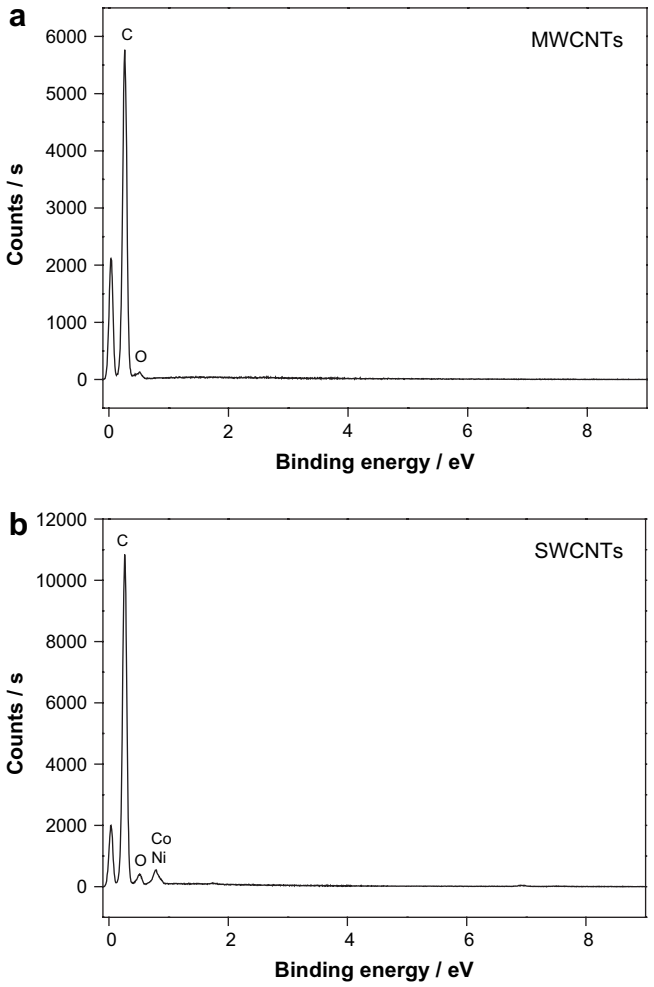

Fig. 2. Energy dispersive X-ray (EDX) spectra of (a) MWCNTs and (b) SWCNTs.

absence of CNTs. There was no precipitation of PNVC in the presence of MeOH. This indicates that the reaction conditions have no effect on the polymerisation of NVC monomers and that CNTs have the ability to promote the *in situ* polymerisation of NVC monomers at an elevated temperature.

The question of how CNT surface initiates the NVC polymerisation and the reaction mechanism is posed. It has recently been established that CNTs are good electron acceptors [9–12,22], while the NVC monomer is a fairly good electron donor [23,24]. Therefore, when the mixture of CNT and NVC was heated at an elevated temperature, NVC donates a single electron to itinerant carbon π^* (anti-bonding orbital) of CNTs [11] and forms an electron deficient active moieties $NVC^{+\bullet}$, which starts the polymerisation process through a well-established pathway [23,24] (initiation → propagation → termination). The tentative mechanism of NVC polymerisation in the presence of CNTs is described in Schemes 1 and 2.

Also interesting is the intensities of the characteristic peaks of PNVC in the case of the PNVC/SWCNT nanocomposites are higher than those of the PNVC/MWCNT nanocomposites (see Fig. 4). This observation indicates that the PNVC content in the case of the PNVC/SWCNT nanocomposites is much higher than that in the PNVC/MWCNT nanocomposites. To support this conclusion, the amount of PNVC formed in the presence of CNTs was measured gravimetrically. Results are summarised in Table 2. The results show that the conversion percentage of NVC to PNVC polymer in the case of the NVC/MWCNTs' polymerisation system is 27, whereas in the case of NVC/SWCNTs' polymerisation system, a 70 percent conversion is observed (see Table 2). This is most probably associated with the huge surface area of SWCNTs, as compared to that of MWCNTs, which actually leads to the high degree of conversion of NVC monomers to PNVC polymers. Based on these results, it can be concluded that the SWCNTs are more efficient in promoting NVC polymerisation than MWCNTs.

The morphology of purified CNTs, PNVC homopolymer and nanocomposite samples was studied by FE-SEM. FE-SEM images are shown in Fig. 5. Fig. 5a is a FE-SEM image of pure MWCNTs. Spherical monodispersed nanoparticles of PNVC with an average diameter of 85 nm are shown in Fig. 5b. The FE-SEM image of the PNVC/MWCNT nanocomposites (Fig. 5c) shows a completely different morphology when compared to that of pure MWCNTs, due to the homogeneous wrapping of the outer surfaces of MWCNTs by PNVC polymer chains and this is more discernible in the high-magnification FE-SEM image as shown in Fig. 5d, [25].

In contrast to the PNVC/MWCNT nanocomposites, PNVC/SWCNT nanocomposites (see Fig. 6) show a completely different morphology where very long and highly entangled SWCNTs form a dense and robust network structure in the PNVC matrix (Fig. 6c). This can clearly be observed in the high-magnification FE-SEM image, Fig. 6d.

In general, it is very difficult for SWCNTs to be well dispersed in a polymer matrix, because of their natural tendency to agglomerate into thick ropes or bundles, as well as their inherent insolubility in most solvents. When the mixture of the NVC/SWCNTs was heated

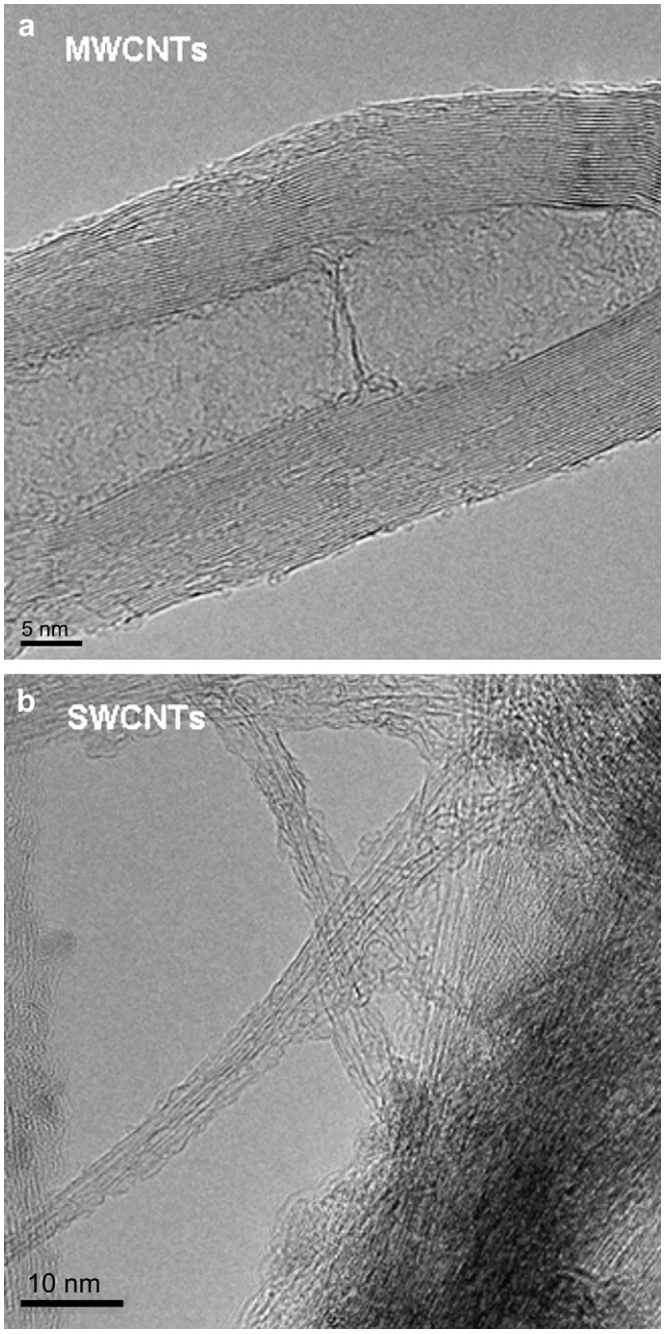

Fig. 3. High resolution transmission electron microscopic (HR-TEM) images of (a) MWCNTs and (b) SWCNTs.

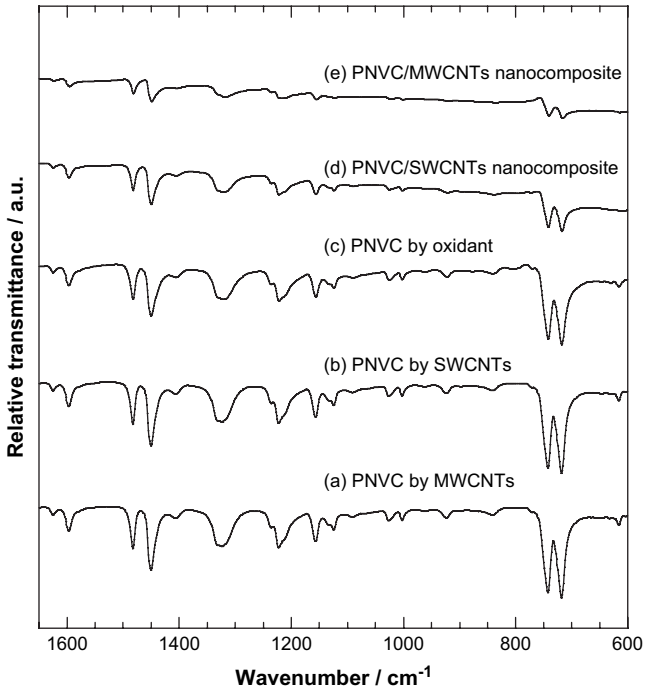

Fig. 4. Attenuated Total Reflectance Fourier transform infrared (ATR-FTIR) spectra of (a) PNVC extracted from PNVC/MWCNTs' nanocomposite, (b) PNVC extracted from PNVC/SWCNTs' nanocomposite, (c) PNVC synthesised by $FeCl_3$, (d) PNVC/SWCNTs nanocomposite, and (e) PNVC/MWCNTs nanocomposite.

above the melting point of NVC, melted NVC monomers first inserted into the SWCNT bundles and started polymerisation on the SWCNT surfaces. Separation of single tubes from the bundles and the formation of a network structure have occurred during the precipitation of the PNVC polymer on the bundles in MeOH.

To understand the different types of morphology in the cases of the PNVC/MWCNT and PNVC/SWCNT nanocomposites, Raman spectroscopic analyses of pure MWCNTs, SWCNTs, and corresponding nanocomposite samples were conducted. Fig. 7 represents the Raman spectroscopic results of pure MWCNTs and its nanocomposite with PNVC. Spectroscopic results revealed that the D-band (defect band) is more intense than the G-band (graphitic band), which indicate that tubes are not homogeneous and have lots of defects on their surfaces. In the case of the nanocomposite sample, the intensities of both bands are decreased. This suggests that the nanocomposite sample needs more energy to vibrate the individual tube or each tube became more bulky. There is also no shift of bands in the case of the nanocomposite sample. This clearly indicates the homogeneous wrapping by the PNVC polymer chains on the MWCNT outer surfaces, without forming any covalent bonds. Further confirmation of wrapping on the MWCNT

Table 1
Observed FTIR characteristic peaks for PNVC prepared by $FeCl_3$, PNVC prepared by CNTs, PNVC/CNT nanocomposites and extracted residue from PNVC/SWCNTs' nanocomposite and along with their probable assignments

Observed peaks (cm^{-1})					Assignments
PNVC by oxidant	PNVC by CNT s	PNVC/MWCNTs' nanocomposite	PNVC/SWCNTs' nanocomposite	Extracted residue from PNVC/SWCNTs' nanocomposite	
718	718	714	717	729	Ring deformation of substituted aromatic structure
741	742	738	741	750	$>CH_2$ rocking vibration
1156	1156	1152	1155	1160	Out of plane deformation of vinylidene group
1322	1323	1312	1322	1330	$>CH_2$ deformation of vinylidene group
1450–1482	1450–1482	1447–1480	1450–1482	1446–1474	Ring vibration of NVC moiety
1625	1625	1622	1625	1620	C=C stretching vibration of vinylidene group

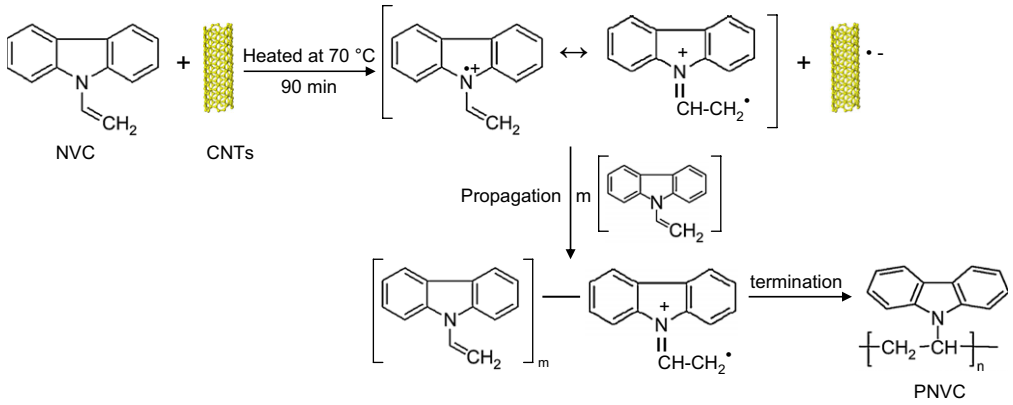

Scheme 1. Tentative mechanism for the *in situ* solid-state polymerisation of NVC monomer by CNTs at an elevated temperature.

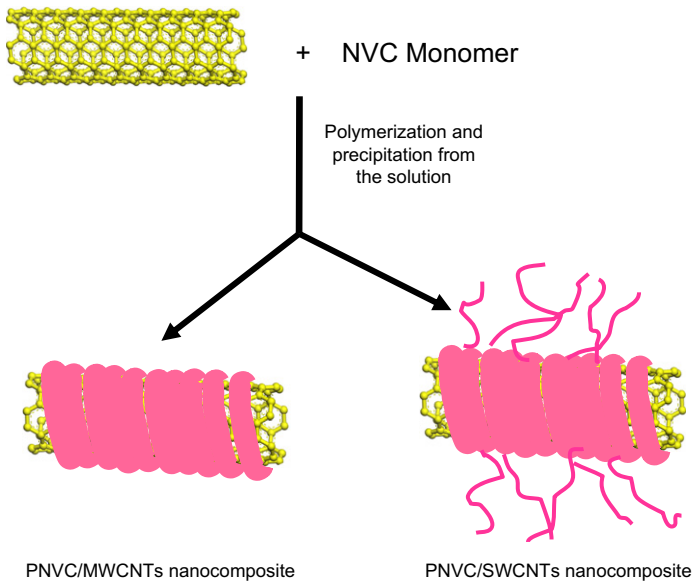

Scheme 2. Schematic view of nanocomposite formation in case of NVC/MWCNT and NVC/SWCNT polymerisation systems.

outer surfaces without forming any covalent bonds with the PNVC polymer was revealed by the recovery of all PNVC polymers from the nanocomposite sample with benzene extraction at 70 °C for 48 h. There is also no appearance of the characteristic FTIR peaks of PNVC from the extracted residue.

The Raman spectroscopic results of pure SWCNTs and the corresponding nanocomposites with PNVC are shown in parts (a) and (b) of Fig. 8, respectively. Like MWCNTs, the surfaces of SWCNTs also show lots of defects. It's interesting to note, however, that in case of the PNVC/SWCNT nanocomposites, not only the intensity of the characteristic Raman bands of SWCNTs was decreased, but band positions also shifted towards a higher wave number region. These observations indicate that SWCNT surfaces were not only coated by PNVC polymer chains, but that some polymer chains were also grafted on the SWCNT outer surfaces.

Table 2
Typical data from NVC/CNTs polymerisation systems

Materials	Weight (g) of			Polymer/CNTs' ratio	Conductivity (S/cm)
	NVC	CNTs	Nanocomposite		
For PNVC/MWCNTs' nanocomposite	0.5	0.05	0.18	2.6	1.0
For PNVC/SWCNTs' nanocomposite	0.5	0.05	0.40	7	3.2×10^{-4}

To confirm the grafting of PNVC chains on the SWCNTs' surface, dry PNVC/SWCNT nanocomposites were repeatedly refluxed (three times) with benzene at 70 °C with continuous stirring for various time intervals (total time was 72 h), untill the extracts did not yield any precipitation of PNVC in MeOH. Finally, the total contents of the system were centrifuged and the centrifugate was separated from the residue. This procedure would remove all ungrafted PNVC from the SWCNT surfaces, but will leave grafted PNVC on the SWCNT surfaces. The residue was then washed thoroughly with boiling MeOH and followed by acetone and overnight dried at 100 °C under vacuum. The dried sample was then used for various characterisations, such as FTIR, Raman, FE-SEM, and XPS studies.

The ATR spectrum of extracted residue from the PNVC/SWCNTs' nanocomposite confirms the presence of PNVC in the extracted residue (see Fig. 9). IR bands and probable assignments are also shown in Table 1. Data from Table 1 clearly support the presence of PNVC polymer chains in the extracted residue. Even more interesting behaviour was observed in the residue with the Raman spectroscope (Fig. 8c), where the position of the characteristic Raman bands remained at the same position as observed in the PNVC/SWCNT nanocomposites, the intensity of all peaks, however, increased significantly. This suggests that grafted PNVC chains still were attached to the CNT outer surfaces. However,

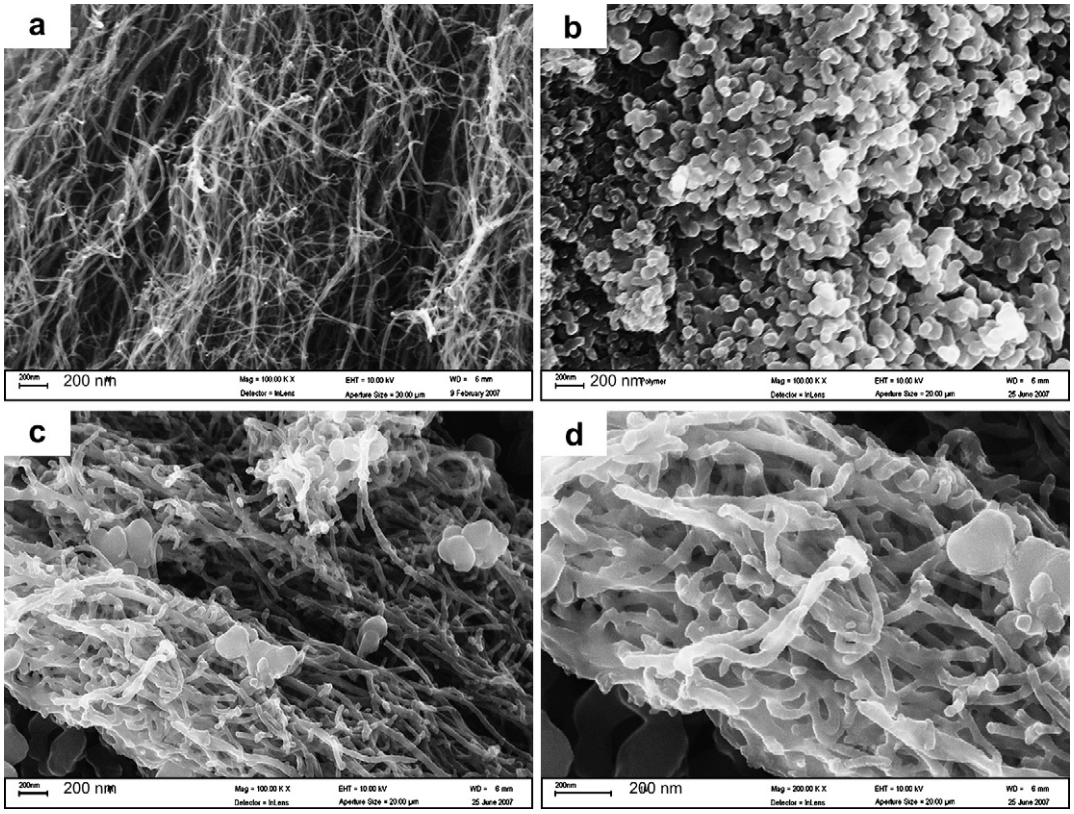

Fig. 5. Field emission scanning electron microscopic (FE-SEM) images of (a) pure MWCNTs, (b) PNVC extracted from nanocomposite, and (c and d) PNVC/MWCNTs' nanocomposite at two different magnifications.

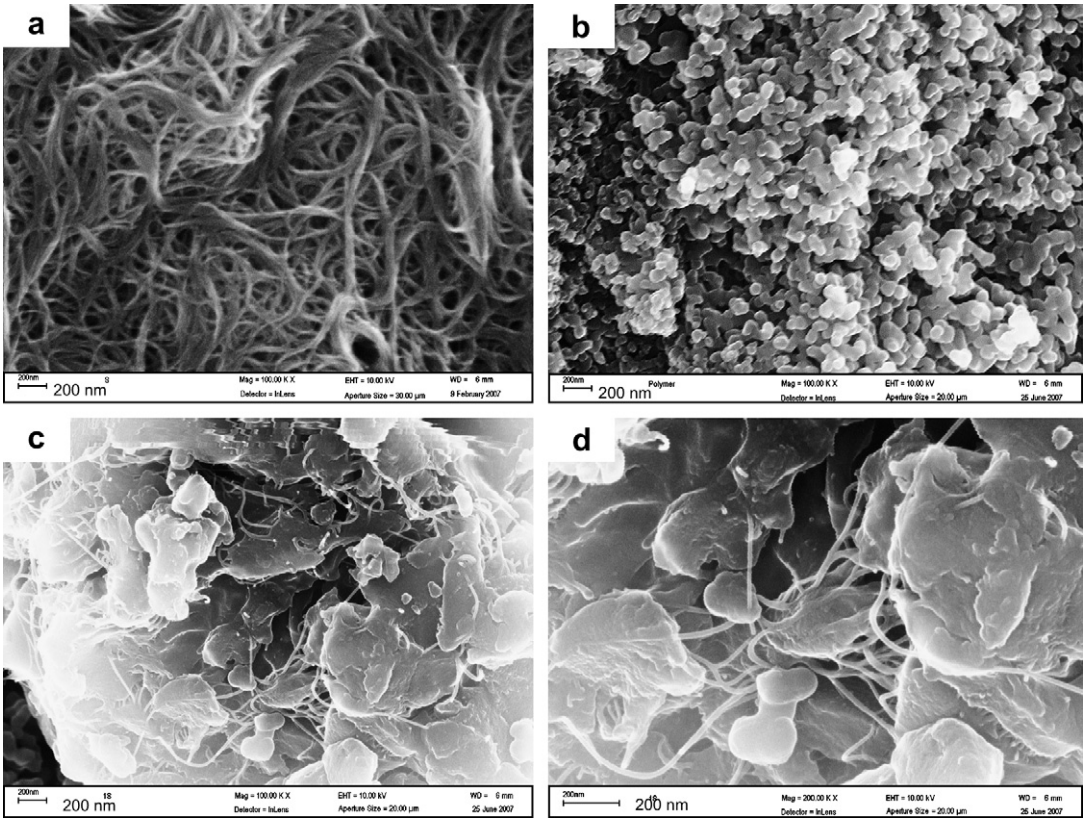

Fig. 6. Field emission scanning electron microscopic (FE-SEM) images of (a) pure SWCNTs, (b) PNVC extracted from nanocomposite and (c and d) PNVC/SWCNTs' nanocomposite at two different magnifications.

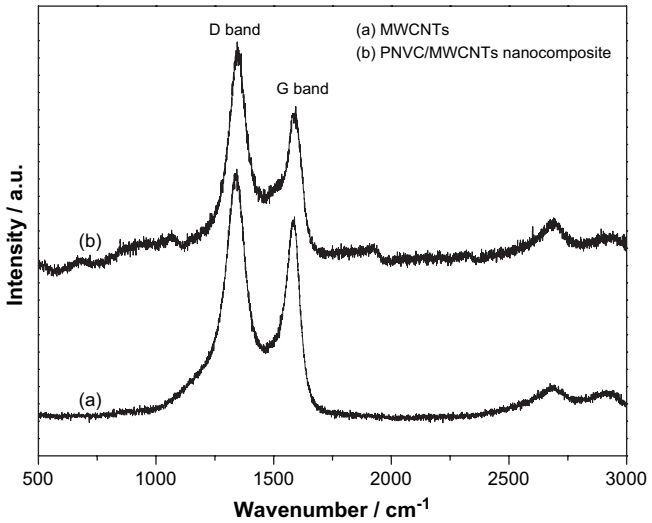

Fig. 7. Raman spectroscopic results of pure MWCNTs and its nanocomposite with PNVC.

the ungrafted PNVC polymer chains were completely removed applying the benzene solution during extraction. To support ATR and Raman spectroscopic results, a FE-SEM analysis of the residue sample was also performed. Results are shown in Fig. 10. It can be seen from Fig. 10 that the morphology of PNVC grafted SWCNTs (b) is completely different from that of pure SWCNTs (a).

To further support the grafting of PNVC chains on the outer surfaces of SWCNTs, XPS analyses were carried out. Fig. 11 shows the XPS results of (a) SWCNT (b) PNVC/SWCNTs' nanocomposite, (c) PNVC prepared by SWCNTs, and (d) extracted residue from the PNVC/SWCNT nanocomposites sample. There is no observed N 1s peak in the case of SWCNTs. The PNVC homopolymer and PNVC/SWCNT nanocomposites show N 1s peak at binding energy of the same position, 398.0 eV for the '–N–' species of the carbazole group [26,27] (see Fig. 11b). This is related to the chemical environment of the N element in pure PNVC and nanocomposites, which is almost the same.

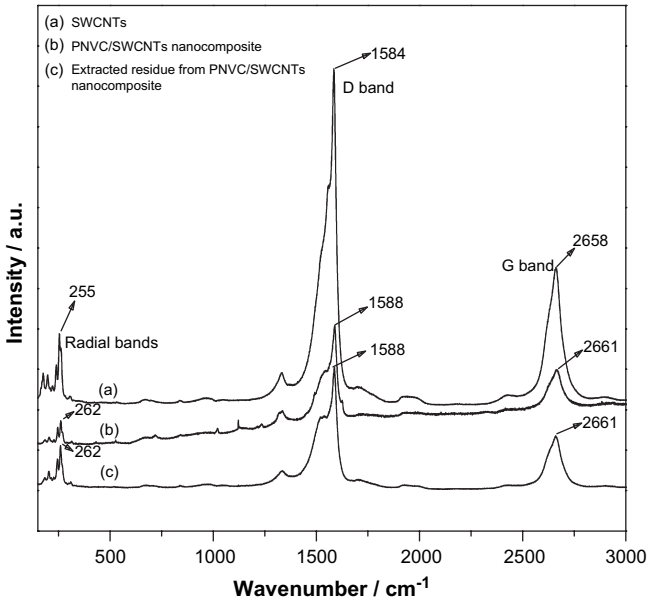

Fig. 8. Raman spectroscopic results of (a) pure SWCNTs, (b) PNVC/SWCNTs' nanocomposite, and (c) extracted residue from PNVC/SWCNTs' nanocomposite. Excitation wavelength was 514.5 nm.

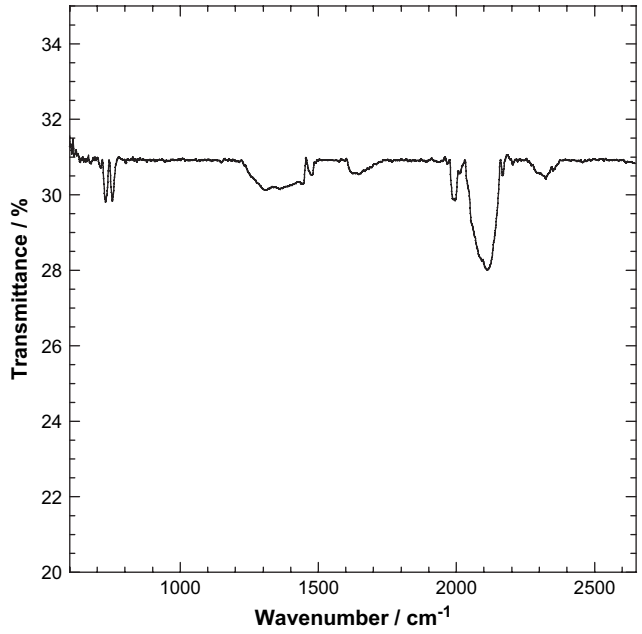

Fig. 9. Attenuated Total Reflectance Fourier transform infrared (ATR-FTIR) spectrum of PNVC/SWCNTs' nanocomposite extracted residue.

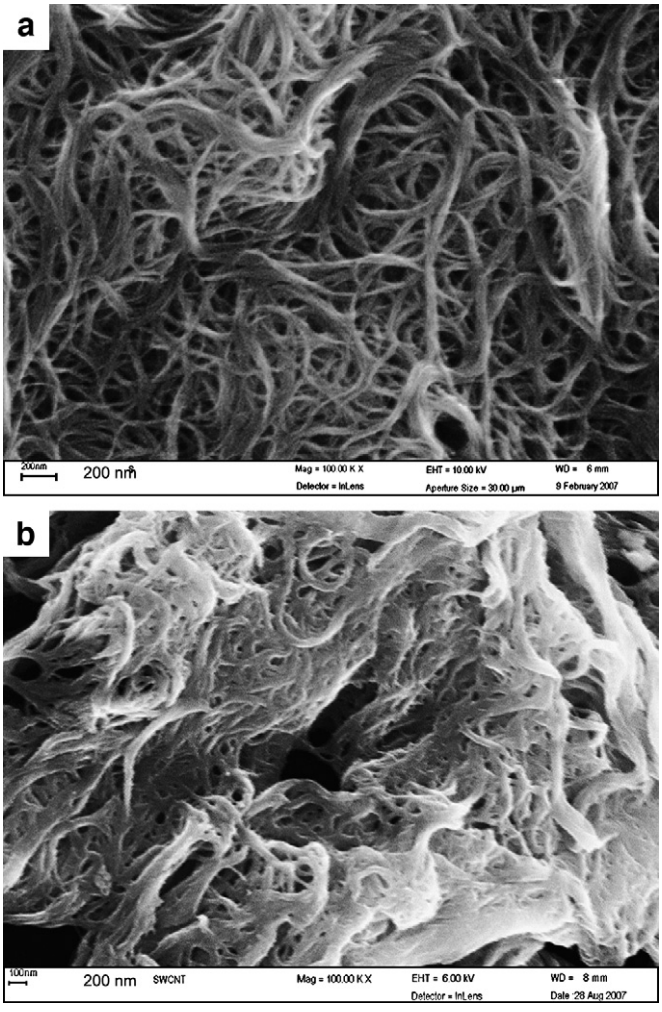

Fig. 10. Field emission scanning electron microscopic (FE-SEM) images of (a) pure SWCNTs, (b) extracted residue.

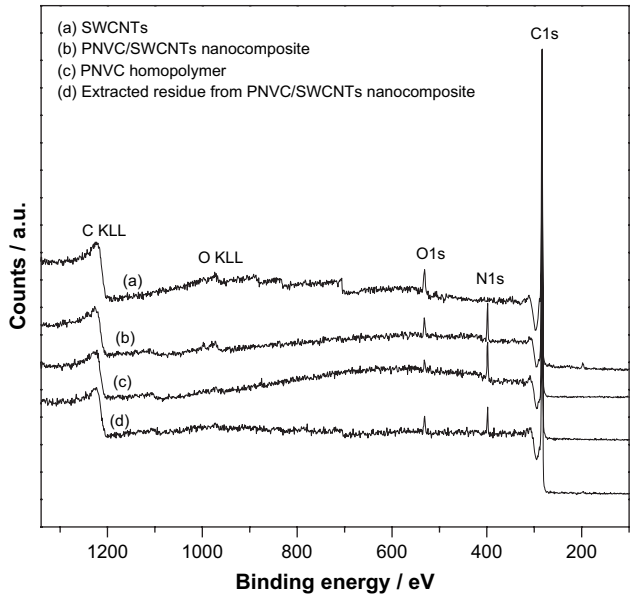

Fig. 11. X-ray photoelectron spectroscopic (XPS) scans of (a) pure SWCNTs, (b) PNVC/SWCNTs' nanocomposite, (d) extracted residue from the PNVC/SWCNTs' nanocomposite, and (c) pure PNVC.

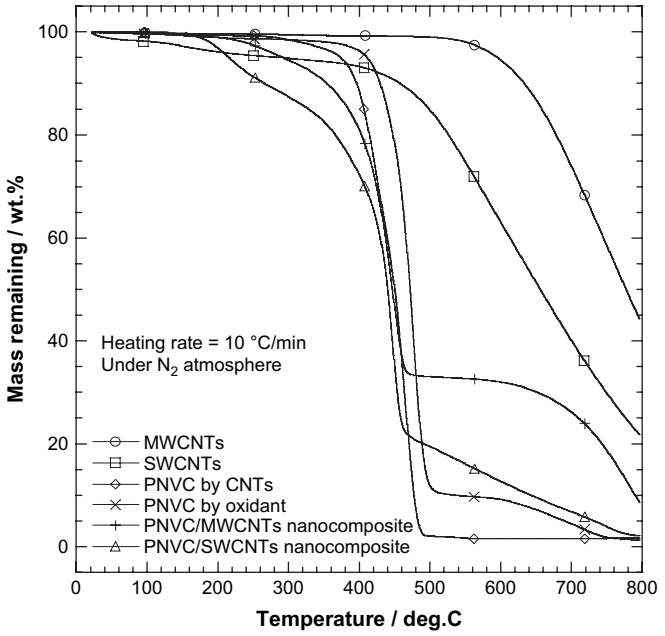

Fig. 12. TGA thermograms of various samples under nitrogen environment. The heating rate was 10 °C/min.

Similarly, in the case of C 1s, the core-level spectra for PNVC and nanocomposites also show peak at 282 eV for the 'C–H/C–C/C–N' species. Extracted residue from the PNVC/SWCNT nanocomposite samples, on the other hand shows two peaks at 282 eV for C 1s and 398 eV for N 1s, and the C/N atomic ratio is 26.05, which is higher than that of PNVC (13.71). This result again supports that some PNVC chains are grafted on the outer surfaces of the SWCNTs during polymerisation. We believe that this type of grafting of the PNVC polymer chains on the CNT surfaces in the case of NVC/SWCNTs' polymerisation system is due to the huge surface reactivity of the SWCNTs' surface to promote the NVC polymerisation as compared to that of the MWCNTs. Details studies are currently undertaken to understand the exact grafting mechanism of PNVC on the outer surfaces of SWCNTs and why two different types of CNTs show different degrees of polymerisation reactivity to NVC polymerisation.

Another interesting behaviour of the nanocomposites manifested in the thermal degradation. Fig. 12 shows the typical TGA traces of weight loss of various samples as a function of temperature under a nitrogen atmosphere. It is evident from Fig. 12 that the thermal stability of MWCNTs is much higher than that of SWCNTs in the entire range of temperatures studied. Although the onset degradation temperature (1.5 wt.% at 304 °C) of both PNVC samples (extracted from the nanocomposite samples or synthesised in the presence of the $FeCl_3$) is the same, however, PNVC synthesised by $FeCl_3$ shows much higher overall thermal stability than that of PNVC extracted from the nanocomposite samples. This may be due to the formation of very high molecular weight polymer chains in the presence of a strong oxidant and/or the impregnation of some 'Fe' ions in the polymer matrix.

In the much higher temperature range (above 500 °C), the degradation behaviour of the PNVC/MWCNT nanocomposites is completely different from the degradation behaviour of the PNVC/SWCNT nanocomposites. This may be due to the different types of structure formation in the case of two different nanocomposites and not only that the overall thermal stability of the PNVC/MWCNT nanocomposites sample is much higher than that of the PNVC/SWCNT nanocomposites. But also due to the much higher thermal stability of MWCNTs than that of SWCNTs.

On the other hand, the lower onset degradation temperature of both nanocomposite samples compared to the pure PNVC sample, may be due to the presence of some unreacted/unwashed monomer or very short polymer chains in the nanocomposites' sample. However, the higher thermal stability of the nanocomposite samples, as compared to PNVC in the higher temperature range (above 500 °C), is related to the presence of much higher thermally stable CNTs.

To understand the effect of CNTs on the electrical property of PNVC, the dc conductivity of the compression moulded samples measured in the four-probe method. The dc conductivity results are shown in Table 2. Interestingly the dc conductivity of pure PNVC sample ($\sim 5.9 \times 10^{-13}$ S/cm) dramatically increased after the nanocomposites preparation with MWCNTs (~ 1.0 S/cm) (average of three independent measurements with a maximum error of 7%). An increase of about 10^{13} fold in the electrical conductivity was observed. The PNVC/SWCNT nanocomposites show the dc electrical conductivity of 3.2×10^{-4} S/cm, an increase of about 10^9 fold. Such a difference in the value of electrical conductivity in the two different nanocomposites sample is due to the presence of a higher amount of MWCNTs in the PNVC/MWCNT nanocomposites or a very high content of non-conductive PNVC in the PNVC/SWCNT nanocomposites (see Table 2). This again supports previous observations that SWCNTs are more efficient to initiate NVC polymerisation than MWCNTs.

4. Conclusion

In this study, we have demonstrated the different degree of efficiency of MWCNTs and SWCNTs to NVC bulk polymerisation. ATR-FTIR studies revealed that under the same experimental conditions, the ability of SWCNTs to initiate the *in situ* polymerisation of NVC monomers was much higher than that of MWCNTs. FE-SEM observations showed two different types of morphology in the case of prepared nanocomposites. A homogeneous wrapping of the outer surfaces of CNTs by PNVC chains was observed in the case of the PNVC/MWCNT nanocomposites, whereas a dense and robust network of very long and highly entangled morphology of CNTs was observed in the case of the PNVC/SWCNT nanocomposites. This

may be due to the different degree of surface reactivity between MWCNTs and SWCNTs.

In general, it is very difficult for the SWCNTs to be well dispersed in the polymer matrix because of their very high tendency to agglomerate into thick ropes or bundles, and their inherent insolubility in most solvents. When the mixture of NVC and SWCNTs was heated above the melting point of NVC, melted NVC monomers first inserted into the SWCNTs' bundle and started polymerisation from the SWCNT surfaces. The separation of some of the tubes from the bundles and the formation of network structure were occurred during the precipitation of the PNVC polymer on the SWCNT bundles in the MeOH solution. Raman spectroscopic results showed that MWCNT surfaces are homogeneously coated by the PNVC polymer. However, in the case of the PNVC/SWCNT nanocomposites some PNVC polymer chains were also grafted on the SWCNT surfaces. ATR-FTIR spectra, FE-SEM observation and XPS studies supported the Raman spectroscopic results. This may be due to the very high degree of activation of the SWCNTs' surface to promote NVC polymerisation and is actually related to the huge surface area of individual SWCNTs. The dramatic improvement of the dc electrical conductivity of the PNVC sample after the nanocomposite formation with MWCNTs as compared to that of SWCNTs is due to the presence of a higher content of highly conductive MWCNTs in the nanocomposite sample or a higher content of nonconductive PNVC in the PNVC/SWCNT nanocomposite sample.

This work provides a new direction for initiating other vinyl monomers and also for fabricating nanocomposites of vinylpolymers with CNTs without adding any external initiator. Ongoing work will focus on establishing the exact polymerisation mechanism and why SWCNTs are more efficient initiators for NVC polymerisation than MWCNTs, the fabrication of plastic solar cells based on the PNVC/CNTs' nanocomposite and measuring the photoconductivity of nanocomposite materials.

Acknowledgements

S. Sinha Ray thanks the CSIR Executive and the Department of Science and Technology, SA, for financial support.

References

[1] Mylnikov V. Adv Polym Sci 1994;115:1.
[2] Biswas M, Das SK. Polymer 1982;23:6423.
[3] Jang J, Nam Y, Yoon H. Adv Mater 2005;21:1382 and references cited therein.
[4] Star A, Stoddart JF, Steuerman D, Diehli M, Boukai A, Wong EW, et al. Angew Chem Int Ed 2001;40:1721.
[5] Coleman JN, Dalton AB, Curran S, Rubio A, Davey AP, Drury A, et al. Adv Mater 2000;12:213.
[6] Wang J, Musameh M, Lin Y. J Am Chem Soc 2003;125:2408.
[7] Chen RJ, Zhang Y, Wang D, Dai H. J Am Chem Soc 2001;123:3838.
[8] Dai L, Soundarrajan P, Kim T. Pure Appl Chem 2002;74:1753.
[9] Sun Y, Wilson SR, Schuster DI. J Am Chem Soc 2001;123:5384.
[10] Riggs JE, Guo Z, Carroll DL, Sun YP. J Am Chem Soc 2000;122:5879.
[11] Rao AM, Eklund PC, Bandow S, Thess A, Smalley RE. Nature 1997;388:257.
[12] Lee RS, Kim HJ, Fisher JE, Thess A, Smalley RE. Nature 1997;388:255.
[13] Wu W, Zhang S, Li Y, Li J, Liu L, Qin Y, et al. Macromolecules 2003;36:6286.
[14] Li C, Liu C, Li F, Gong Q. Chem Phys Lett 2003;380:201.
[15] Wu W, Zhang S, Li Y, Li J, Liu L, Qin Y, et al. Macromolecules, in press.
[16] Kim JY, Kim M, Choi JH. Synth Met 2003;139:565.
[17] Wu W, Liu L, Yanga L, Guo ZX, Dai L, Zhu D. Chem Phys Lett 2002;364:196.
[18] Wang W, Lin Y, Sun YP. Polymer 2005;46:8634.
[19] Baibarac M, Lira-Cantu M, Oro SJ, Baltog I, Casan-Pastor N, Gomez-Romero P. Compos Sci Technol 2007;67:2556.
[20] Maity A, Sinha Ray S, Pillai S. Macromol Rapid Commun 2007;28:2224.
[21] Ellinger LP. Polymer 1964;5:559.
[22] Zengin BH, Zhou W, Jin J, Czerw R, Smith Jr DW, Echegoyen I, et al. Adv Mater 2002;14:1480.
[23] Sinha Ray S, Biswas M. Synth Met 2003;132:213.
[24] Ballav N, Maity A, Biswas M. Mater Chem Phys 2004;87:120.
[25] Kim ST, Choi HJ, Hong SM. Colloid Polym Sci 2007;285:593.
[26] Ling QD, Lim SL, Song Y, Zhu CX, Chan DSH, Kang ET, et al. Langmuir 2007; 23:312.
[27] Beamson G, Briggs D. High-resolution XPS of organic polymer – the scienta ESCA300 database. Chichester, England: Wiley; 1992. p. 224.